Reinforcement effects and safety monitoring index for high steep slopes
A case study in China

Lin, Chaoning; Li, Tongchun; Zhao, Lanhao; Zhang, Zhe; Lin, Chuan; Liu, Xiaoqing; Niu, Zhiwei

DOI
10.1016/j.enggeo.2020.105861

Publication date
2020

Document Version
Final published version

Published in
Engineering Geology

Citation (APA)
Lin, C., Li, T., Zhao, L., Zhang, Z., Lin, C., Liu, X., & Niu, Z. (2020). Reinforcement effects and safety monitoring index for high steep slopes: A case study in China. *Engineering Geology*, *279*, Article 105861. https://doi.org/10.1016/j.enggeo.2020.105861

Engineering Geology 279 (2020) 105861

Contents lists available at ScienceDirect

Engineering Geology

journal homepage: www.elsevier.com/locate/enggeo

Reinforcement effects and safety monitoring index for high steep slopes: A case study in China

Chaoning Lin [a,b], Tongchun Li [a,*], Lanhao Zhao [a], Zhe Zhang [d], Chuan Lin [c], Xiaoqing Liu [a], Zhiwei Niu [a]

[a] College of Water Conservancy and Hydropower Engineering, Hohai University, Nanjing 210098, Jiangsu, China
[b] Faculty of Technology, Policy, and Management, Delft University of Technology, Delft 2628, BX, the Netherlands
[c] College of Civil Engineering, Fuzhou University, Fuzhou 350108, Fujian, China
[d] Shandong Survey and Design Institute of Water Conservancy, Jinan 250000, Shangdong, China

ARTICLE INFO

Keywords:
Steep slope
Reinforcement
Stability analysis
Safety monitoring index
Field monitoring
Anti-shear tunnels

ABSTRACT

High and steep slopes which have developed fractures and intercalations are a great threat to the operation of dams and reservoirs. In this work, the geological conditions and potential modes of failure of the slope found in the right bank of Suofengying hydropower station are investigated for the slope stability and the results are presented. In order to strengthen the slope, an innovative stabilization scheme is employed. The stabilization techniques include development of anti-shear tunnels, anti-slide piles, anchor cables, concrete support structure, etc. Further, the slope stability and reinforcement effects using various stabilization techniques are studied by using finite element strength reduction method. Moreover, in situ monitoring is carried out and the data obtained is analyzed. From the results, it is observed that the deformations that are detected using multipoint extensometers have decreased after the installation of remedial reinforcements. From the analysis of remedial reinforcement methods, it is found that the most critical reinforcement is the development of anti-shear tunnels. In order to monitor the stresses in stirrups and the propagation of cracks in the anti-shear tunnels, three levels of safety monitoring index are proposed. The safety monitoring index is developed based on the results obtained by the simulation of the process of failure of the reinforced slope. The developed safety monitoring index is further applied to the Suofengying project in order to evaluate the overall stability of the slope. The results obtained by monitoring indicate that the performance of the reinforcement structures is satisfactory and the slope has better stability. The methodology proposed in this work shall be useful for similar projects to obtain stability of slopes.

1. Introduction

In the last few decades, a series of large-scale hydropower projects have been constructed in southwest China. These projects involve a series of ultra-high, ultra-large and complex slopes, such as the side slopes (H = 170 m) of the five-step ship lock in the Three Gorges hydropower station (Fan et al., 2015), the left-bank slope (H = 200 m) in the Baihetan hydropower station (Xu et al., 2018), the rock slope (H = 250 m) of the spandrel groove in the Xiluodu hydropower station (Sun and Hu, 2007), and the slope (H = 300 m) in the Xiaowan hydropower station (Chen et al., 2016). Most of the hydropower projects are constructed in mountainous regions which have poor geological and geotechnical conditions with fractures, shear zones, etc.(Yu et al., 2014). In their banks, the instability of the slope is one of the key issues that have to be considered during design process, construction and operation of dams and reservoirs.

There is a wide variety of slope failures which is commonly known as landslides. Such failures depend on the material involved, the morphology, the rate of movement, the triggering mechanisms and type of run-out. Several researchers have carried out studies in this area of research (Hungr et al., 2014; Stead and Wolter, 2015; Varnes, 1978). The failures of slopes can be classified into four main categories based on the type and degree of movement of the slope during failure such as fall, topple, slide and flow. Fall refers to the free-fall movement of material from a steep slope or cliff. Topple is similar to fall, however it involves a pivoting action rather than a complete separation at the base of the failure. Slide refers to a mass movement over a well-defined surface in which the relative displacements are concentrated. Finally flow refers to

* Corresponding author.
E-mail addresses: linchaoning@hhu.edu.cn (C. Lin), tcli@hhu.edu.cn (T. Li).

https://doi.org/10.1016/j.enggeo.2020.105861
Received 30 March 2020; Received in revised form 7 August 2020; Accepted 11 October 2020
Available online 22 October 2020

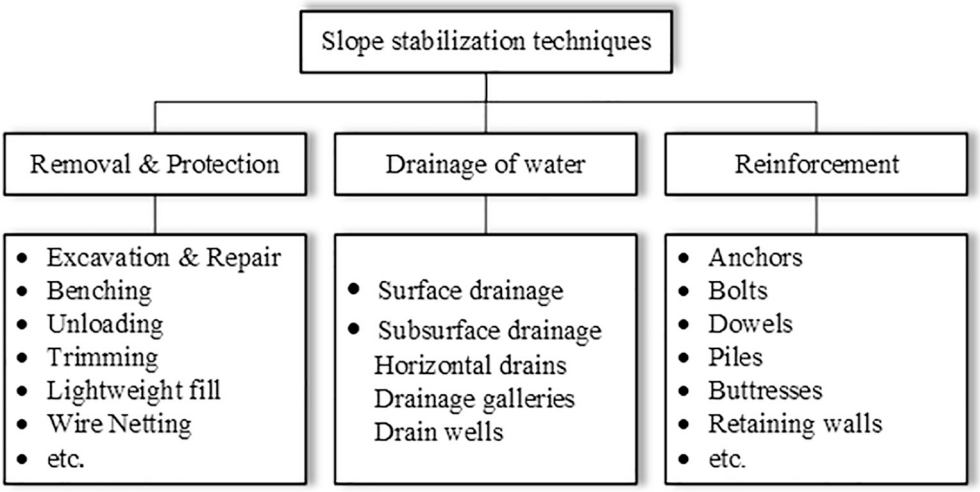

Fig. 1. Categories of slope stabilization techniques.

a fluidized mass behavior in which water and air are involved.

Failure of large slopes is a serious threat to human lives, the infrastructures in the banks and the hydropower station that is situated beside it (Macfarlane, 2009). For instance, the enormous slide of mass of rocks and debris into the Vajont reservoir in 1963, provoked a giant wave which made the dam overflow and destroyed several nearby villages (Kilburn and Petley, 2003; Paronuzzi and Bolla, 2012). Similarly, the Qianjiangping landslide which occurred after the first stage of impoundment of the Three Gorges reservoir in 2003 resulted in several deaths and a direct economic loss of 7 million USD (Wang et al., 2004). Therefore, a safe management system of hydropower projects in mountainous regions is essential and requires preventive measures that have to be taken in order to control the occurrence of slope failures.

Modem methods of design and stabilization of rock slopes were developed since 1970s (Brawner and Wyllie, 1976; Fookes and Sweeney, 1976) and are continuously being refined and developed (Abramson et al., 2001; Chen et al., 2016; Wyllie and Norrish, 1996). Fig. 1 illustrates some common stabilization techniques divided into three categories namely removal and protection, drainage of water and development of reinforcements (Fig. 1). The selection of the appropriate stabilization technique is very important and should be selected based on the geological conditions of the site. The slope at the Huangjinping hydropower station that was empirically designed with anchor cables of lengths 40 m to 45 m was found insufficient to stabilize the slope. However the remedial design of anchor cables with a length of 100 m was found to successfully stabilize the slope (Chen et al., 2017). In the right bank slope of Dagangshan hydropower station, anti-shear tunnels were used for enhancing the overall shear resistance and reinforcement was carried out in the slope at six different elevations (Ma et al., 2017). In the left abutment slope of Jinping I hydropower station, a combined reinforcement system with pre-stressed cables and three shear-resistant concrete plugs were utilized in order to effectively restrain the slope deformation and ensure the slope stability during construction (Li et al., 2015).

From various studies, it was found that structural control plays a very important role in large slope instabilities. Due to the complexity of reinforced slopes, it is difficult to evaluate the stability of reinforced slopes using theoretical methods. Therefore, numerical methods such as Finite Element Method (FEM) have been used in many complex slope problems (Böhme et al., 2013; Griffiths and Lane, 1999). In FEM, the shear strength reduction method (SSRM) is usually adopted in order to compute the critical strength reduction factor (SRF) (Dawson et al., 1999; Zienkiewicz et al., 1975). When the slope reaches the ultimate failure state, the critical SRF is referred as the Factor of Safety (FOS) (Griffiths and Marquez, 2007). In addition to FEM, Finite Difference Method (FDM) (Soren et al., 2014), Discrete Element Method (DEM) (Firpo et al., 2011), Rigid Body Spring Element Method (RBSM) (Zhang et al., 2001), Discontinuous Deformation Analysis Method (DDA) (Sun et al., 2011) and other such analytical methods (Bhandary et al., 2019; Dadashzadeh et al., 2017; Ureel and Momayez, 2014) have been used and applied successfully in many engineering practices.

Apart from the numerical simulation methods, the field monitoring is an effective method that can be used in slope safety management. In field monitoring method, the actual slope is visually inspected. Traditional measurement techniques using instruments such as total stations, multipoint extensometers, crack meters and laser scanner are useful for monitoring the deformation of slopes. Moreover, instruments such as stress meters, strain gauges, and micro seismic monitoring systems have been developed for monitoring the stress distribution of slopes and their reinforcement structures. The data obtained by monitoring provides a reliable base for the assessment of safety of slopes. (Wu et al., 2011) evaluated the stability of the slope in the Three Gorges reservoir area with the data collected using ground surface displacement monitoring, deep displacement monitoring and underground water monitoring. (Zhu et al., 2015) investigated the stability condition of a reinforced model slope using the fiber-optic monitoring network.

In this work, Suofengying hydropower station is considered and the studies are carried out. Suofengying hydropower station is located in the mountainous regions in the western part of China. The main water-retaining structure is a gravity dam. The Dr2 slope is one of the most dangerous parts at Suofengying hydropower station. The instability of the slope will directly affect the water intake. It further affects the central control room and some of the other hydraulic equipments at the right bank. The wave propagation may lead to a dam failure or a dam overtopping. The geological and geotechnical conditions based on in situ surveys of the Suofengying hydropower station are presented. The potential modes of failure are investigated and different remedial techniques such as anti-shear tunnels, anti-slide piles, anchor cables, grouting treatment, etc. are studied to stabilize the slope. Further, a 3D finite element model is created to analyze the behavior of the reinforced slope. In this model, rock mass, fractures, intercalations and reinforcement structures are taken into consideration. SSRM is introduced in order to analyze the efficiency of the stabilization method used for the Dr2 slope.

Monitoring index is used to provide warning and it plays an important role in the slope safety management. Generally, the monitoring index is determined based on the data collected using displacement monitoring, because they can reflect the characteristics of the slope

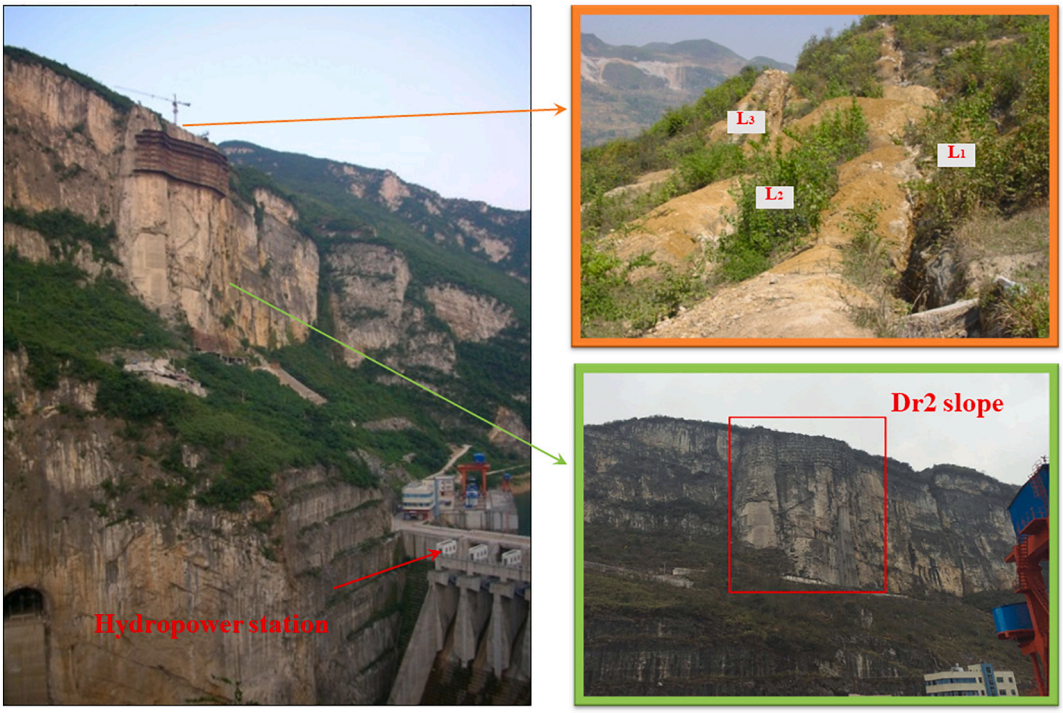

Fig. 2. The location of the Dr2 high steep slope.

intuitively. If the observed displacements are unacceptably large or no longer follow the previous trend of data, then the slope is considered to be unstable. However, in view of the small magnitude of deformation of the slope after reinforcement (the maximum displacement detected by the multipoint extensometers is 2.12 mm), it might not be the best solution to determine overall safety monitoring index via displacement monitoring data. In addition, a project is usually equipped with a large number of monitoring instruments. If plenty of monitoring items are involved in the safety monitoring index, the management would be cumbersome and inefficient. Therefore, we should focus on the critical and vulnerable parts of the project. For the reinforced slope project like the Dr2 slope in Suofenying hydropower station, the reinforcement structures would fail first before the failure of the overall slope. Furthermore, it is proposed to determine the safety monitoring index of the slope by analyzing the working status of the critical reinforced structures. Based on the progressive failure process identified by the numerical analysis, three levels of safety monitoring index are proposed to determine the condition of operation of the eight anti-shear tunnels and to provide an early warning if the reinforced slope is under abnormal conditions.

2. Overview of the project

The Suofengying hydropower station is located on the mainstream of

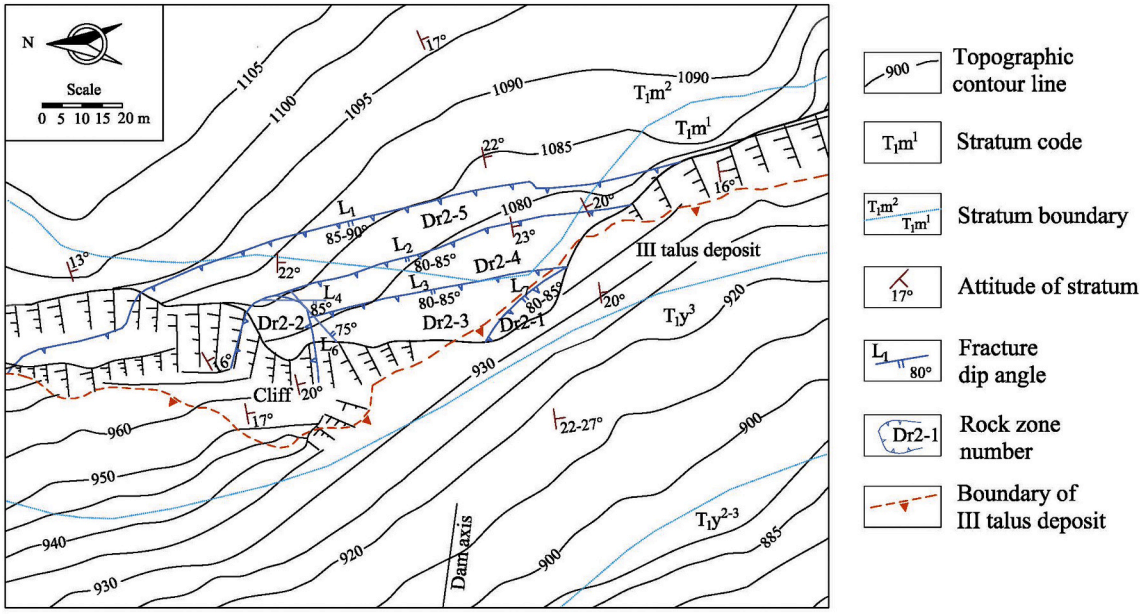

Fig. 3. Geological map of the Dr2 slope.

Table 1
Physical and mechanical parameters of the Dr2 slope.

Stratum	Lithology	Bulk density (g/cm^3)	Young's modulus (GPa)	Poisson ratio	Shear strength	
					f	*c* (MPa)
T_1m^2	Thin-bedded dolomite and muddy dolomite	2.68	5	0.32	0.65	0.6
T_1m^1	Medium-thick limestone and dolomitic limestone	2.68	5	0.3	0.7	0.7
T_1y^3	Mudstone and silty mudstone	2.67	2	0.32	0.45	0.3
T_1y^{2-3}	Dolomitic limestone	2.69	10	0.25	1	1
J_1,J_3,J_4		2.65	1.5	0.35	0.35	0.01
J_2		2.65	1.5	0.35	0.3	0.01
L_1		1.8	0.125	0.35	0.35	3e-5
III talus deposit		2	1.5	0.3	0.4	0.01
Interface of III talus deposit with T_1y^3 and T_1y^{2-3}		2	1.5	0.3	0.4	0.015
Backfill material (C15 concrete) of L_1, L_2 and L_3		2.3	15	0.2	0.7	0.3

the Wujiang River in Qianxi County, China. The capacity of the hydropower station is 600,000 KW. The Dr2 slope is located above the limestone cliff on the right side of the dam abutment (Fig. 2). The dimensions of the slope are 180 m in length, 200 m in height and 29–37 m in width. The upper and middle parts of the slope are composed of thin-bedded to medium-thick grey limestone and dolomitic limestone (T_1m). The lower part of the slope is composed of grayish-green and purplish-red mudstone intercalated with muddy limestone (T_1y^3). At the toe of the rock cliff, there is a talus slope named the III talus deposit which is 20–50 m deep. The slope is large in scale and complex in structure.

2.1. Geological conditions of Dr2 slope

The Dr2 high steep slope is located above the limestone cliff on the right side of the dam abutment. The crest and bottom elevations of the Dr2 slope are 1080 m and 880 m, respectively (Fig. 4). It is narrower in the upper part and wider in the lower part. The total volume of the rock mass is about 785,000 m^3. Above an elevation of 1070 m, there is a gentle slope platform with a slope of 5–10°and is composed of dolomite (T_1m^2). The surface of the platform is distributed by alluvial clay and gravel upto a thickness of 0.5–1 m. There is a talus deposit with a slope of 24–40° in the part below the elevation of 960 m. In between the elevations of 960 m and 1070 m, there is a steep cliff with a slope of over 70° and it is composed of limestone (T_1m^1). The attitude of the Dr2 slope is N75–85°E and SE∠12–25°. The dip angle of the T_1m stratum which comprises of the upper and the middle parts (T_1m^1 and T_1m^2) ranges between 12° and 17°. The dip angle of the T_1y^3 mudstone stratum ranges between 15° and 25°.

Seven major fractures (L_1–L_7) are developed and the outcrops of the fractures are shown in Fig. 3. The Dr2 rock mass is separated from an integral mass of rock due to the fracture L_1. It forms the back edge of the Dr2 slope and has a large separation ratio of 90% in the plane. L_1 is the largest fracture of the seven fractures with a length of 130 m and the crack opening of 0.2–1.0 m. Fractures L_2 and L_3 are located at the outer side of L_1. Fractures L_4 and L_6 are located at the downstream side of the slope. Further fractures L_5 and L_7 are located at the upstream side of the slope.

In addition to the fractures, there are three main mudded intercalations namely J_1, J_2 and J_3 that are developed in the T_1y^3 mudstone stratum. The thickness of J_1 is 20 cm and the components include purplish-red mudstone and grey-white mudstone which are mostly softened. There is an obvious indication in J_1 that an intercalated sliding has occurred. The thickness of J_2 is 10 cm and the filling materials include grey-green debris with a small amount of clay. The thickness of J_3 ranges from 2 cm to 5 cm and the main components in it are debris and mud. Further, there is a mudded intercalation J_4 which is developed in the T_1m^1 limestone stratum. The thickness of J_4 ranges from 10 cm to 20 cm and the main components include the debris and mud.

Based on the distribution of fractures, the rock slope is divided into five parts, namely Dr2-1, Dr2-2, Dr2-3, Dr2-4 and Dr2-5 (Fig. 3). The physical and mechanical parameters of the Dr2 slope are given in Table 1, in which *c* represents the cohesion and *f* represents the friction coefficient, respectively. The geological conditions of the slope were investigated using comprehensive methods such as drilling, adit exploring and geophysical prospecting. The material properties were determined by tests.

2.2. Failure modes

Based on the analysis of the geological conditions of Dr2 slope, two potential failure modes namely the toppling failure and the shear sliding failure are identified. The different types of failures are briefly described below.

2.2.1. Toppling failure

The main part of the Dr2 slope is a steep cliff with a slope of over 70°. Moreover, the three main fractures (L_1, L_2 and L_3) cut the slope into thin pillars of thickness 15–20 m each. Therefore, the most possible failure modes include the overall toppling failure and the local toppling failure.

Overall toppling failures occur due to the gravity load of the slope, which is applied to the soft rock base, T_1y^3 mudstone. This causes compressive deformation in the rock base. The main causes of the overall toppling failures include activities such as excavation, blasting, external water pressure, weathering of mudstone, etc. Local toppling failures occur due to the deterioration of mechanical properties of the slope.

2.2.2. Shear sliding failure

In addition to the fractures and the intercalations, the soft rock base bears the heavy load of the 200 m high rock pillar. Therefore, the slope suffers from local damages and discontinuous breakage zones. They may also suffer shear sliding failure along the sliding surface which comprises of the leading edge which is formed by the weak intercalation, the trailing edge which is formed by the fracture L_1 and some adverse structural planes in the mudstone stratum.

2.2.3. Stabilization works

In order to avoid such failures and to stabilize the slope of the Suofengyin hydropower station, several preventive measures were implemented. The typical section of the reinforced slope is shown in Fig. 4. In order to control the toppling deformation, pre-stressed anchor cables and anchor rods were installed at the top and the upper part of the slope to integrate the rock masses. Similarly, to avoid the shear slide, measures such as anti-slide piles and anti-shear tunnels were installed in the middle and lower parts of the slope. The details of the stabilization measures are briefed below.

C15 concrete was used to fill the fractures L_1, L_2 and L_3 in order to strengthen the rock mass. The fractures at the top were sealed by the concrete material in order to prevent the rainwater from flowing into the fractures and to reduce erosion. A concrete patand was installed at the top of the slope, and forty seven anchor cables which were pre-stressed with pre-stressing forces of 1000 kN were installed on the patand. The lengths of the anchor cables installed ranges between 18 m and 52 m. Further, an intercepting drain was placed at the top of the slope in order

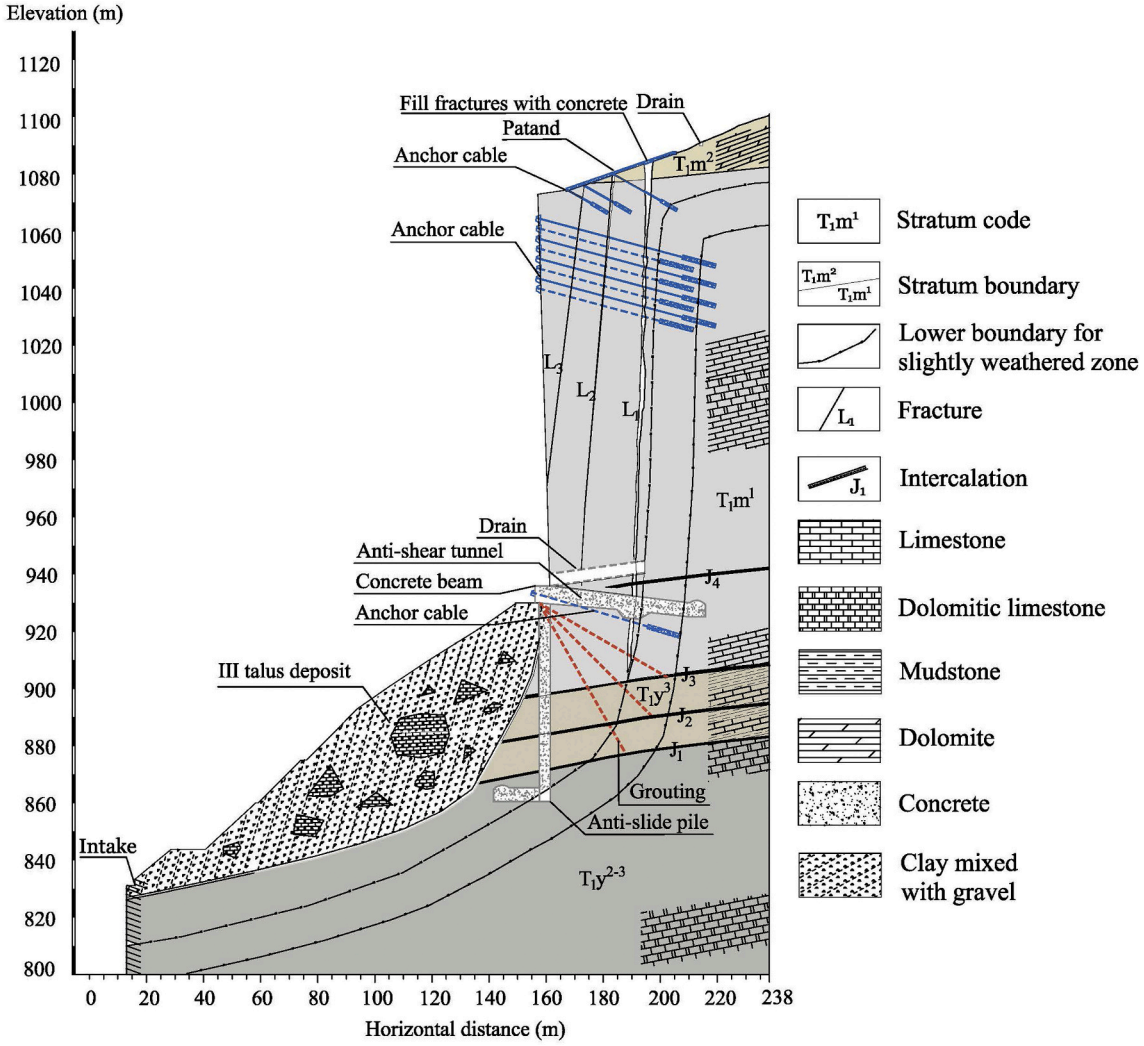

Fig. 4. Geological section of the reinforced Dr2 slope.

to prevent the surface runoff from flowing into fractures.

In the upper part of the slope, one hundred and seventy six anchor cables which were pre-stressed with pre-stressing forces of 2000 kN were installed at an elevation of 1040–1060 m in order to strengthen the rock cliff. Among the anchor cables, half of them are 49 m in length and the other half of them are 35 m in length. Furthermore, a set of long anchor rods was installed on the rock cliff at an elevation of 970–1060 m. The installed anchor rods are 36 mm in diameter, 12 m in length and the spacing between the rods is 2.5 m. Further, the external surface of the rock cliff was treated with wire netting and shotcrete at an elevation of 970–1060 m.

In the middle and the lower parts of the slope, a construction platform was built at an elevation of 930 m in order to provide a foundation for the reinforcement work. A row of eight horizontal anti-shear tunnels was constructed in the T_1m^1 limestone stratum at an elevation of 930 m and filled with C20 concrete. Once the construction of tunnels #8 and #6 was completed, the excavation of the tunnel #1 was started. During the excavation process, it was found that the exposed mudstone stratum was higher than the estimated amount. However, as per the geological identification, the location of the tunnel #1 was already in the T_1y^3 mudstone stratum. Therefore, the construction of tunnel #1 was stopped and the remaining tunnels were redesigned. Tunnels #1–#8 were constructed perpendicular to the fracture L_1. The cross-section of the tunnels #2 to #5 and #7 is 4.6 m × 4.0 m, and the cross-section of their intersection portion with the fracture L_1 is 4.6 m × 7.5 m (Fig. 5). Similarly, the cross-section of the tunnels #1, #6 and #8 is 3.5 m × 4.0 m and the cross-section of the intersection with the fracture L_1 is 3.5 m × 7.5 m. The dimension of the opening of the fracture L_1 at the intersection ranges from 5 cm to 50 cm.

Furthermore, a row of six vertical anti-slide piles was placed in the T_1y^3 mudstone stratum. The upper parts of the piles are embedded into the T_1m^1 limestone stratum and the lower parts are embedded into the T_1y^{2-3} dolomitic limestone stratum. The piles were constructed using C20 concrete. The diameter of each pile is 6 m and the length ranges from 60 m to 80 m. A reinforced concrete beam was used to connect the piles and tunnels to the construction platform. The reinforced concrete beam is about 100 m long, 8 m wide and 3.42 m high. Moreover, twenty anchor cables of length 45 m, which were pre-stressed with pre-stressing forces of 2000 kN, were installed on the beam. On this basis, a combined reinforcement system of tunnels, piles and anchor cables were formed (Fig. 5). A concrete support structure was constructed above the concrete beam in order to stabilize the overhanging rock mass in the Dr2-1 area. The support structure is 65 m high and the cross-section of the structure at the bottom is 10 m × 12 m. Moreover, the internal fractures in T_1y^3 mudstone were treated with cement grouting.

2.2.4. *Reinforcement effects*

The Dr2 slope was reinforced by various types of techniques which include anchor cables, anti-shear tunnels, anti-slide piles, etc. The effectiveness of the different reinforcement techniques and their

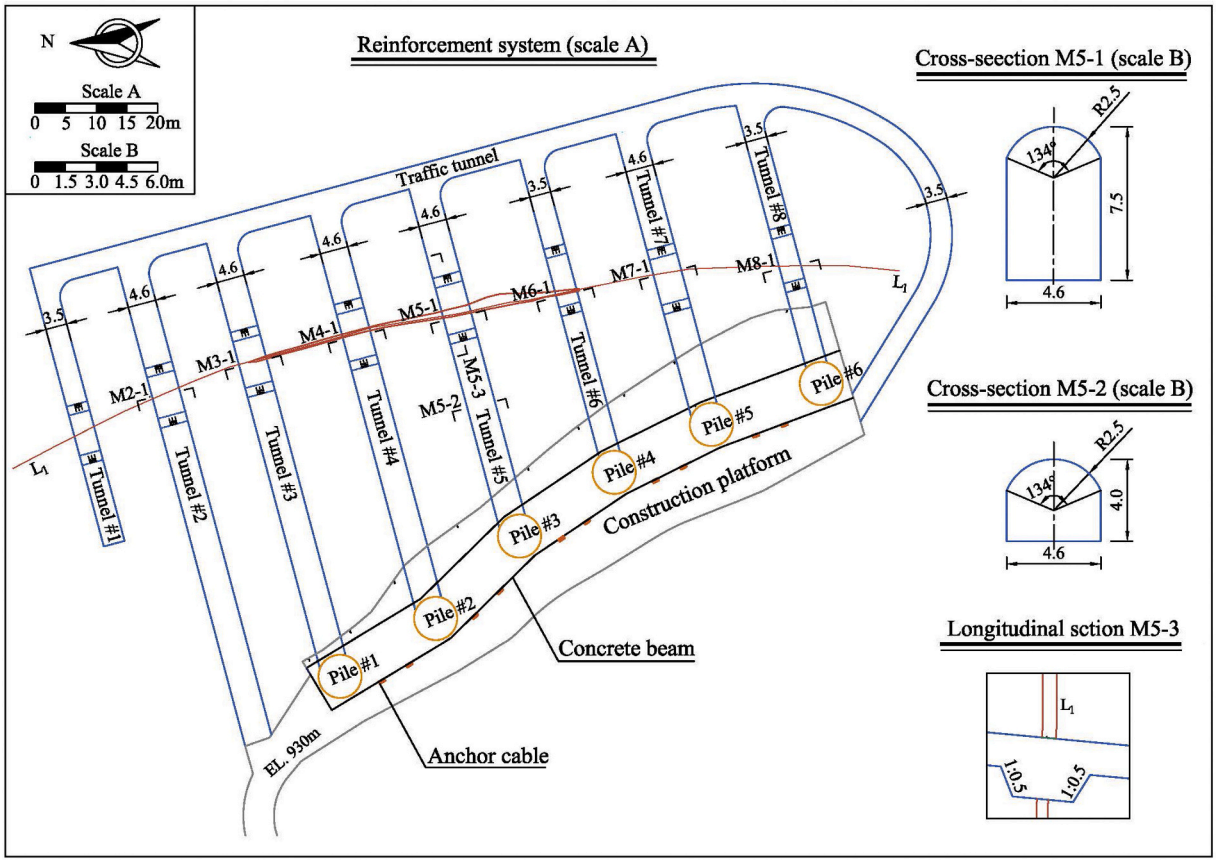

Fig. 5. Schematic diagram of the reinforcement system at EL. 930 m (Unit: m).

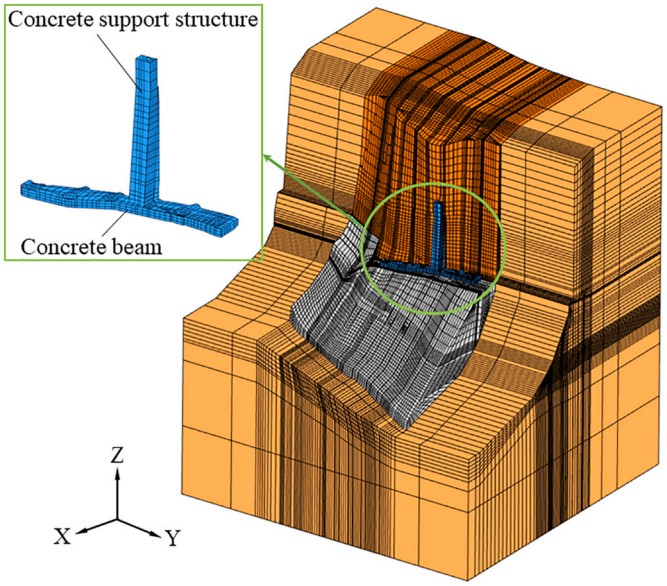

Fig. 6. Finite element mesh of the 3D model.

combinations are analyzed using a 3D numerical model. The finite element method (FEM) and the shear strength reduction method (SSRM) are used to calculate the factor of safety (FOS) of the slope under different conditions.

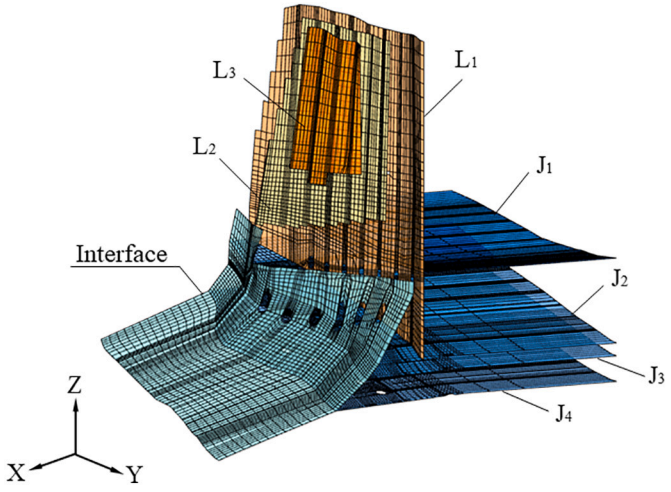

Fig. 7. Finite element mesh of the weak structural planes (Fractures L_1–L_3, Intercalations J_1–J_4, and the Interface).

2.3. Finite element modeling

Finite element schematizations of the Dr2 slope and reinforcement structures are carried out based on the exploration and construction data (Fig. 6). The length of the model is 340 m in X-direction, 350 m in Y-direction and 390 m in *Z*-direction. These dimensions are taken at elevations from 690 m to 1080 m). Further, the model is meshed into 263,152 elements.

The schematizations of weak structural planes are shown in Fig. 7, including three main fractures (L_1,L_2,L_3), four weak intercalations (J_1,

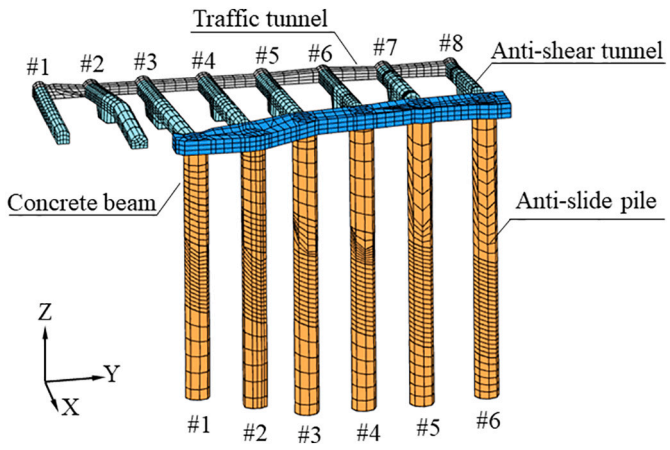

Fig. 8. Schematic representation of the finite element mesh model of the anti-shear tunnels and the anti-slide piles.

J_2, J_3, J_4), and the interface between rock slope and III talus deposit. The weak structural planes which include the three fractures, four intercalations and the interface are simulated by using thin-layer elements. The rock mass, fractures and intercalations are modeled using Mohr-Coulomb model. The material properties used during the simulation are shown in Table 1.

Models with reinforcement structures such as anti-shear tunnels, anti-slide piles, anchor cable systems, grouting treatments and the support structures are described as follows. While modeling the anti-shear tunnels and anti-slides, the following procedure is followed. The schematic description of the eight anti-shear tunnels and the six anti-slide piles are shown in Fig. 8. In Fig. 8, the tunnels #2–#8 are extended to the construction platform. The ends of the eight tunnels are connected by a traffic tunnel which is backfilled with concrete at the end of construction. The tunnels and the piles are connected using a concrete beam, which forms a combined reinforcement system of tunnels and piles. The material used for the tunnels and piles construction is C20 concrete. C20 concrete is assumed to be linear-elastic in the simulation. The density, Young's modulus and Poisson ratio are taken as 2.5 g/cm^3, 28 GPa and 0.167, respectively.

The model of the anchor cable system consists of three parts. The first part consists of forty seven anchor cables which are pre-stressed with pre-stressing forces of 1000 kN. It is located at the top of the slope and is further connected to the top ground beam. The second part consists of one hundred and seventy six anchor cables which are pre-stressed with pre-stressing forces of 2000 kN. It is located at the upper part of the slope. The third part consists of twenty anchor cables that are pre-stressed with pre-stressing forces of 2000 kN. It is located on the construction platform at an elevation of 930 m. The anchor cables are modeled using beam elements. The anchoring force is equally interpolated and is applied to the nodes of the finite element model in order to simulate the effectiveness of the anchor cables.

Then, further modeling is carried out assuming that the grouting treatment is completed in the T_1y^3 mudstone stratum. Therefore, the Young's modulus, Poisson ratio, friction coefficient and cohesion of the T_1y^3 mudstone stratum are taken as 1.575G Pa, 0.3, 0.52 and 0.315 MPa, respectively.

Finally, modeling of the support structures is carried out (Fig. 6). While modeling, the bottom of the concrete support structure is connected to the anti-slide pile #4. The material properties of the concrete support structure are the same as the properties used for the tunnels and the piles.

2.4. Analysis

The external forces such as winds, rain and human activities affect the physical and mechanical parameters of the slope. This would result in sliding of the slope. Most reinforcement techniques such as anti-shear tunnels and anti-slide piles work only when the slope has a sliding tendency. In this study, SSRM is used to calculate the FOS of the reinforced slope under different conditions (Table 2). Based on the obtained results, the effectiveness of different reinforcement techniques and their combinations are evaluated and the results are compared. The analysis is carried out in two parts. In the first part, the simulation of the initial stress state of the slope under gravity is carried out. Based on the results obtained, the FOS is calculated for different conditions in the second part.

Table 2
The FOS of the Dr2 slope under different conditions.

Conditions	Reinforcement techniques	FOS	Values added to FOS
i	Natural condition	1.050	0
ii	Grouting treatment for the T_1y^3 stratum	1.058	0.008
iii	47 sets of pre-stressed anchor cables at the top	1.061	0.011
iv	176 sets of pre-stressed anchor cables at the upper part	1.093	0.043
v	Six anti-slide piles	1.149	0.099
vi	Eight anti-shear tunnels	1.124	0.074
vii	Combined reinforcement system of tunnels, piles and anchor cables at the construction platform	1.205	0.155
viii	Concrete support structure and combined reinforcement system at the construction platform	1.211	0.161

The groundwater conditions are not considered in the simulation as the saturation line of groundwater is lower than the bottom elevation of the Dr2 slope. Therefore, it has negligible influence on the slope stability.

In SSRM, the strength parameters of a slope are reduced by a certain factor and the finite element stress analysis is computed. This process is repeated for different values of the strength reduction factor (SRF) until the model becomes unstable. The reduction factor which is obtained when the slope reaches the ultimate failure state is defined as the FOS.

During the analysis, the Mohr-Coulomb criterion is used in which the strength reduction factor K can be expressed as:

$$\tau = (c + \sigma tan\varphi)/K = c_e + tan\varphi_e \quad (1)$$

$$tan\varphi_e = (tan\varphi)/K \quad (2)$$

$$c_e = c/K \quad (3)$$

where c and tanφ represent the cohesion and friction coefficient, respectively; c_e and tanφ_e represent the reduced cohesion and friction coefficient, respectively; and σ and τ are the normal stress and shear stress on the slide surface, respectively.

According to Eqs. (1), (2) and (3), the strength parameters of the rock mass, the fractures and the intercalations are reduced simultaneously and systematically. The described model is implemented in a finite element code (GeHoMadrid). GeHoMadrid is a research software which has been jointly developed between Madrid University (Spain) and Hohai University (China) (Fernandez Merodo et al., 1999). The key issue in the analysis of slope stability using SSRM is determination of the critical unstable status. There are three main criteria for determination of slope instability. They are the non-convergence of the calculation, the abrupt increase of displacement and the development of the plastic zone from the foot to the top of the slope. In this study, due to the differences in the reinforcement types, different instability criteria are used for different conditions listed in Table 2.

For conditions i, ii, iii and iv, there are no reinforcement techniques used in the middle and lower parts of the slope. Therefore, the status of

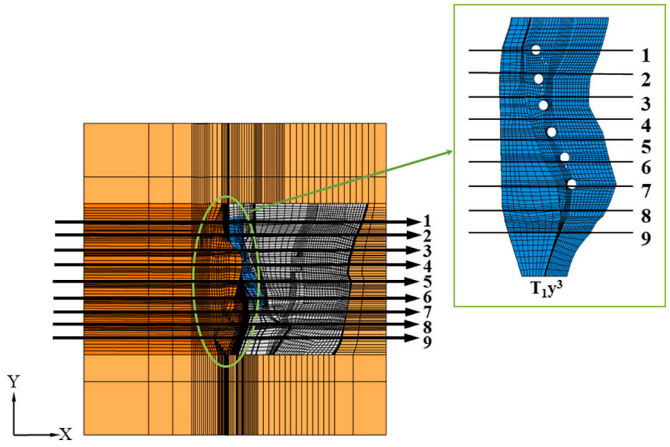

Fig. 9. Typical sections of the Dr2 slope (vertical view).

T_1y^3 mudstone stratum is primarily considered as the strength of the material is low in this region. Moreover, there are weak intercalations in this region which may form a sliding surface. In the analysis, nine critical sections are selected in order to observe the degree of instability at different sections in each step of the SSRM. The locations of the critical sections coincide approximately with the locations of anti-shear tunnels and anti-slide piles (Fig. 9). The FOS of each critical section is determined by the abrupt increase of the node displacement in the finite element model of T_1y^3 mudstone stratum. When more than half of the sections have slipped, it is assumed that the slope has lost its stability. Hence, the FOS of the fifth sliding section is taken as the FOS of the overall slope.

For conditions v, vi, vii and viii, anti-shear tunnels and anti-slide piles are used as reinforcement techniques in the T_1y^3 mudstone stratum. Therefore, it is considered that the FOS depends on load-carrying capacities of piles and tunnels. This inturn decided on the stability of the slope. In this analysis, the finite element internal force method is used to calculate the tension, shear and bending moment of piles and tunnels under different SRF. Further, the failure process of the piles and the tunnels are evaluated based on their load-carrying capacities. A tunnel or a pile is considered to fail if the load exceeds its load-carrying capacity. If more than half of the tunnels or the piles fail, then it is assumed that the slope has lost its stability. Hence, the SRF under this condition is determined as the FOS.

3. Results and discussion

Based on the analysis, the results are obtained under different conditions and the results are presented in Table 2. Further, the estimated FOS values are compared. According to the Chinese specification for the design of engineering slope in water resources and hydropower projects SL386-2007, the required FOS for the slope in this study has to be 1.15 to 1.20. The FOS value of the Dr2 slope obtained in the natural condition is 1.050. It is observed that the obtained FOS value is lesser than the required value.

From Table 2, it is further observed that the FOS values increase after the reinforcement. This indicates that the reinforcement techniques have effectively stabilized the slope. From the analysis, it is observed the application of grouting treatment and the installation of the anchor cables can strengthen the rock mass. Moreover, the installed anti-shear tunnels can enhance the shear resistance of the slope and also control the deformation and thereby prevent crack opening. It is further observed that the anti-slide piles that are constructed in the T_1y^3 mudstone stratum can enhance the stiffness of the slope base. By comparing the results under various conditions, it is observed that while using anti-slide piles, the deformation of the reinforced slope base is minimal when the slope destabilizes at the ultimate state.

The results of various reinforcement techniques are compared and it is found the anti-slide piles are most effective in overall stabilization of the slope. The next effective reinforcement technique is the anti-shear tunnels followed by the grouting treatment. Further, it is observed that the anchor cables at the upper part contribute to better stability than the anchor cables at the top of the slope. It is also observed that, piles and tunnels provide the maximum contribution towards the slope stability. However, from the results, it is found that a single reinforcement is not sufficient to improve the stability of the slope as the FOS values are lesser than 1.15. Therefore, it is necessary to combine the reinforcement in order to provide good stability to the slope. It is observed that the combination of the reinforcement techniques as in the conditions vii and viii (Table 2) results in larger FOS values, which are greater than the required FOS value of 1.20. The FOS increases by 14.8% with combination of reinforcement system of tunnels, piles and anchor cables as in case vii (Table 2) and increases by 15. 3% with the combination of reinforcement system of tunnels, piles, anchors and the concrete support structure as in case viii (Table 2). Therefore, it is concluded that the safety of the slope can be assured with the proposed stabilization method.

3.1. Determination of safety monitoring index for the Dr2 slope

In this section, the progressive failure process of the reinforced slope is studied and discussed. For the reinforced slope project like the Dr2 slope in Suofenying hydropower station, the reinforcement structures should fail before the failure of the overall slope. Therefore, the safety monitoring index of the Dr2 slope should be determined based on the evaluation of the critical reinforcement structures. From the numerical analysis, it is found that the control factor of the overall slope stability is the anti-shear tunnel system as the failure of the slope begins with the failure of the anti-shear tunnels. Therefore, three levels of safety

Table 3
The shear force of tunnel cross-sections in the computational process (Unit: KN).

SRF	Anti-shear tunnel						
	#2	#3	#4	#5	#6	#7	#8
1.190	72,865	71,194	54,863	45,373	19,655	4792	-36,796
1.205	**79,169**	**75,069**	57,994	48,563	22,219	5340	-35,076
1.266	–	–	70,388	60,713	31,561	13,650	-26,403
1.282	–	–	**74,755**	64,494	35,301	16,647	-24,304
1.333	–	–	–	73,102	42,794	21,411	-18,769
1.351	–	–	–	**76,031**	45,472	25,847	16,765
1.429	–	–	–	–	55,720	40,647	6860
1.449	–	–	–	–	**57,979**	42,918	6952
1.639	–	–	–	–	–	70,697	20,150
1.667	–	–	–	–	–	**75,451**	23,956
1.887	–	–	–	–	–	–	51,393
1.923	–	–	–	–	–	–	**57,301**

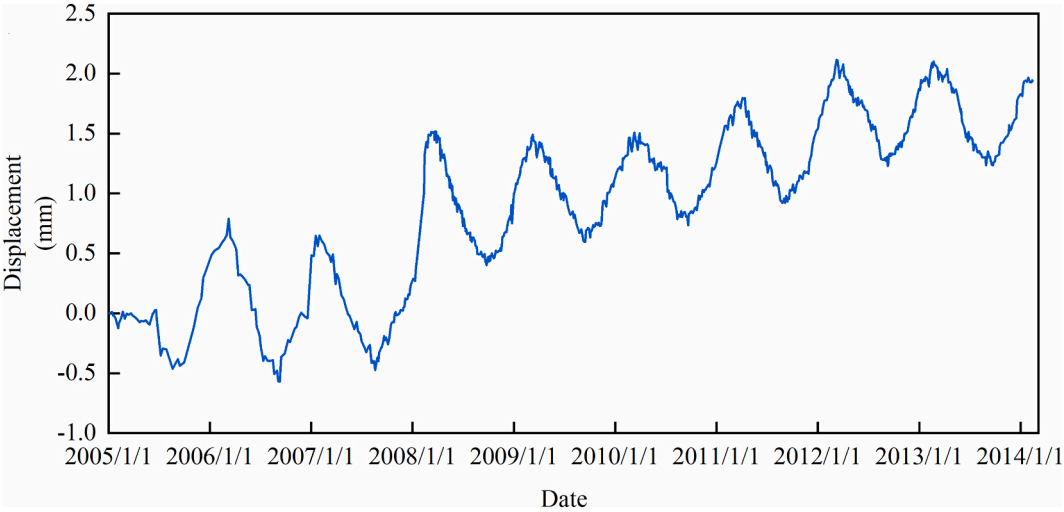

Fig. 10. The measured displacement of MDr2-4-2 at the top of the slope.

monitoring index are proposed by monitoring the condition of anti-shear tunnels.

3.2. The progressive failure process

Based on the analysis results, it is found that the bearing capacity of the slope mainly depends on the load-carrying capacities of anti-slide piles and anti-shear tunnels. Therefore, the shear carrying capacity and the flexural capacity of anti-slide piles and anti-shear tunnels are focused.

During this study, the construction of the tunnel #1 was stopped in the middle of the excavation. Therefore only tunnel #2–#8 are considered in the calculation. In the calculation, when the SRF value reaches 1.205, shear failure occurs in the tunnels #2 and #3. The failure positions are found at the cross-sections M2-1 and M3-1 (Fig. 5). Meanwhile, the remaining tunnels and piles still have a sufficient load-carrying capacity which allows the slope to continue to maintain the stability. When the SRF value reaches 1.351, the shear failure occurs in the tunnels #4 and #5. The failure positions are observed at the cross-sections M4-1 and M5-1 (Fig. 5). More than half of the tunnels fail in this condition. From the results, it is found that the remaining tunnels are not sufficient to provide the required shear carrying capacity for the entire slope. Therefore, it is concluded that the shear failure of anti-shear tunnels is a critical factor for the slope instability. As a result, the FOS of the overall reinforced Dr2 slope is considered to be 1.351.

The progressive failure process of anti-shear tunnels is presented in Table 3. The shear carrying capacity of the cross-sections of tunnels #6 and #8 is 55,973 KN, and the shear carrying capacity of other tunnels is 73,564 KN. The shear force which exceeds the shear carrying capacity of the tunnel cross-section is shown in bold in the Table 3. It is observed that the failure of the tunnels occurs in the sequence of tunnels #2, #3, #4, #5, #6, #7, #8. It is further observed that the tunnels #2 and #3 fail simultaneously during the computational process.

3.3. Three levels of safety monitoring index

In Suofengyin project, a number of instruments, including thermometers, multipoint extensometers, benchmarks, joint meters, stress meters, soil pressure gauges, are embedded inside and around the slope in order to monitor the temperatures, displacements and the other characteristics of the reinforced slope. The monitored data provides a reliable base for slope safety management. Displacement is one of the critical indicators that can intuitively reflect the safety status of a reinforced slope during the construction period. There are six multipoint

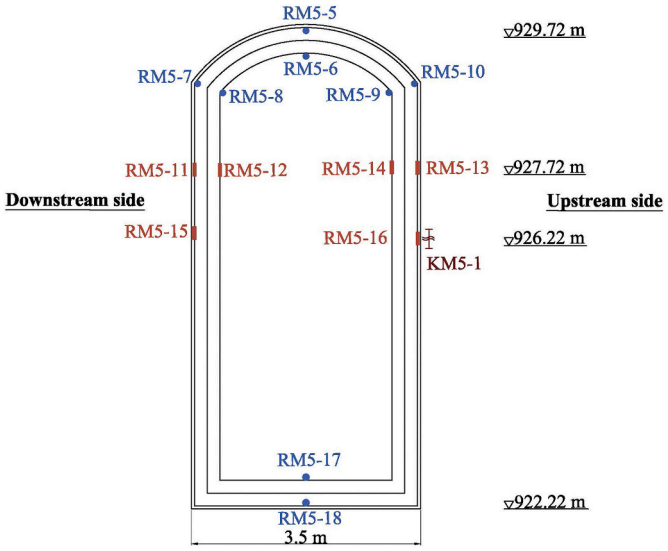

Fig. 11. The arrangement of stress meters and joint meters in tunnel #5 (the cross-section M5-1).

extensometers installed at the top of the slope and four multipoint extensometers installed on the cliff surface at the elevation of 970–1061 m. During the construction period (2005–2013), the slope displacement varied periodically with seasons. The maximum measured displacement of the slope is 2.12 mm. The measured displacements of MDr2-4-2 (located at an elevation of 1081 m) in various period are shown in Fig. 10. From Fig. 10, it is observed that the slope displacement gradually increases from the years 2005 to 2013. After installation of anti-slide piles, anti-shear tunnels and other remedial reinforcement measures which were completed in 2013, the stability of the slope is observed to be improved and the deformations measured by the multi-point extensometers have converged. The slope displacements are relatively low when compared with the annual variations of 0.6–1 mm.

Monitoring indexes are usually determined in order to provide warning and is very essential in ensuring slope safety. In this study, it is proposed to determine safety monitoring index of the overall reinforced slope by determining the working status of critical reinforcement structures.

According to the identified failure process of the Dr2 slope, the vulnerable parts are the intersections of the fracture L_1 and tunnels and

Table 4
The stress meters for monitoring the stress in stirrups.

Anti-shear tunnel	Stress meter 1	Stress meter 2	Stress meter 3	Stress meter 4	Stress meter 5	Stress meter 6
#2	–	–	–	–	–	–
#3	RM3-7	RM3-8	–	–	–	–
#4	RM4-11	RM4-12	RM4-13	RM4-14	RM4-15	RM4-16
#5	RM5-11	RM5-12	RM5-13	RM5-14	RM5-15	RM5-16
#6	–	–	–	–	–	–
#7	RM7-7	RM7-8	RM7-9	RM7-10	RM7-11	RM7-12
#8	–	–	–	–	–	–

Note: There is no stress meter installed in tunnels #2, #6 and #8.

Table 5
The joint meters for monitoring the fracture L_1.

Anti-shear tunnel	Joint meter 1	Joint meter 2
#2	KM2-1	–
#3	KM3-1	–
#4	KM4-1	KM4-2
#5	KM5-1	–
#6	–	–
#7	–	–
#8	–	–

Note: There is no joint meter installed in tunnels #6–#8.

the failure pattern is the shear failure. Therefore, the stress in stirrups and the opening of the fracture is focused. Stress meters are used to monitor the stress in stirrups of tunnel cross-sections. Stirrups are a type of transverse reinforcement installed in concrete tunnels to resist the shear (Ali et al., 2006). A tunnel is considered to have failed if the reading of either of the stress meters reaches 80% of yield stress of stirrups. The yield stress value of the stirrups is 300 MPa. In addition, joint meters are used to monitor the opening of fracture L_1.

Typical arrangements of stress meters and joint meters in tunnel #5 are shown in Fig. 11. Among the stress meters, RM5-11–RM5-16 are used to monitor the stirrup stress. The key stress meters and joint meters in the eight tunnels are listed in Table 4 and Table 5. The stress meters and joint meters were pre-installed in the tunnels during the construction period. The signal from the measuring instruments is transmitted to the external digital panel by wires. Before each measurement, there are procedures for instrument calibration and accuracy check.

The failure process is divided into three stages namely the normal operation stage, the partial plastic yield stage and the failure stage. Correspondingly, the safety monitoring index can be determined as Grade one, Grade two and Grade three. Grade one provides a clear indication of the beginning of the yield and crack in the tunnel system. The monitored values of key stress meters installed in the tunnel #3 reach 80% of the yield stress of the stirrup, and the monitored values of key joint meters installed in the tunnels #2 or #3 abruptly increase.

Grade two indicates the expansion of the yield and cracking zone in the tunnel system. The monitored values of key stress meters installed in the tunnel #4 reach 80% of the yield stress of the stirrup, and the monitored values of key joint meters installed in the tunnel #4 abruptly increase.

Grade three indicates that the tunnel system has failed. The monitored values of key stress meters installed in the tunnels #5 reach 80% of the yield stress of the stirrup, and the monitoring values of key joint

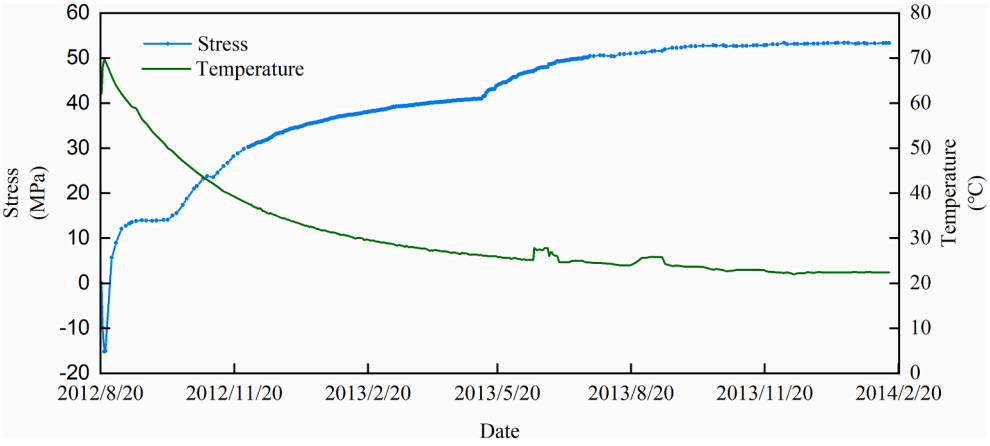

Fig. 12. The stirrup stress measured by RM5-14 in tunnel #5.

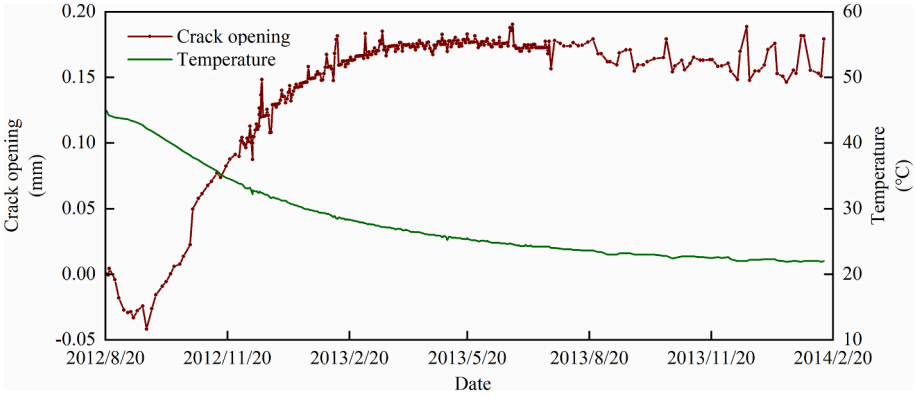

Fig. 13. The opening of fracture L_1 measured by KM5-1 in tunnel #5.

meters installed in the tunnels #5 abruptly increase. The occurrence of the Grade three state should be avoided during the operation stage.

In the initial operation period of anti-shear tunnels, the stress in the stirrup increases rapidly and then gradually stabilizes when the temperature drops from 50 °C to 20 °C. The readings measured using the stress meters listed in Table 5 are found to be less than 70 MPa. Typically measurements of the stirrup stress using RM5-14, during the period from 20 August 2012 to 13 February 2014, is shown in Fig. 12. Moreover, the readings obtained using the joint meters shows that the opening of the fracture tends to be constant. Fig. 13 illustrates the opening of fracture L_1 measured by KM5-1. The monitored results confirm that the slope performs well after the reinforcement techniques are implemented.

4. Conclusion

The stability of the Dr2 high steep slope is a crucial geological engineering problem in Suofengying hydropower station, China. In this study, the failure modes of the slope are investigated and various types of stabilization measures used to address the slope stability problem are presented. The effectiveness of different reinforcement techniques is evaluated using SSRM. The progressive failure process and final failure pattern of the reinforced slope are analyzed and discussed. Based on the results, three levels of safety monitoring index are proposed in order to assist safety management. The conclusions are as follows:

(1) Based on the analysis of geological conditions of the Dr2 slope, the two potential failure modes are identified to be the toppling failure and the shear sliding failure. Various types of reinforcement techniques are adopted in order to enhance the rock mass and prevent the development of fractures. After the installation of the remedial reinforcements, the slope deformations are found to be negligible which indicates the stability of the slope.
(2) The efficiency of different reinforcement techniques is analyzed using a 3D numerical model. From the analysis, it is found the anti-slide piles contribute the most to the slope stability followed by the anti-shear tunnels. From the results, it is concluded that the combined system of reinforcement measures can effectively improve the overall stability of the slope.
(3) From the numerical analysis, it is determined that the shear failure of anti-shear tunnels is the critical factor of overall slope instability. The proposed principle of determining safety monitoring indexes of reinforced slopes based on the performance of reinforcement structures is rational and practical and can be used for evaluating slope safety in similar engineering projects.

Declaration of Competing Interest

The authors declare that they have no known competing financial interests or personal relationships that could have appeared to influence the work reported in this paper.

Acknowledgements

This research has been greatly supported by the National Key Research and Development Plan (No. 2018YFC0407102). Project of the research on long term monitoring and safety evaluation of concrete dams based on BIM (DJ-ZDXM-2018-02).

References

Abramson, L.W., Lee, T.S., Sharma, S., Boyce, G.M., 2001. Slope Stability and Stabilization Methods. John Wiley, USA.
Ali, M.M., Oehlers, D., Seracino, R., 2006. Vertical shear interaction model between external FRP transverse plates and internal steel stirrups. Eng. Struct. 28 (3), 381–389.
Bhandary, R., Krishnamoorthy, A., Rao, A.U., 2019. Stability analysis of slopes using finite element method and genetic algorithm. Geotech. Geol. Eng. 37 (3), 1877–1889.
Böhme, M., Hermanns, R.L., Oppikofer, T., Fischer, L., Bunkholt, H.S., Eiken, T., Pedrazzini, A., Derron, M.H., Jaboyedoff, M., Blikra, L.H., 2013. Analyzing complex rock slope deformation at Stampa, western Norway, by integrating geomorphology, kinematics and numerical modeling. Eng. Geol. 154, 116–130.
Brawner, C., Wyllie, D., 1976. Rock slope stability on railway projects. Am. Railway Eng. Assoc. Bull. 77 (656), 449–474.
Chen, Z., Wang, Z., Xi, H., Yang, Z., Zou, L., Zhou, Z., Zhou, C., 2016. Recent advances in high slope reinforcement in China: Case studies. J. Rock Mech. Geotech. Eng. 8 (6), 775–788.
Chen, T., Deng, J., Sitar, N., Zheng, J., Liu, T., Liu, A., Zheng, L., 2017. Stability investigation and stabilization of a heavily fractured and loosened rock slope during construction of a strategic hydropower station in China. Eng. Geol. 221, 70–81.
Dadashzadeh, N., Duzgun, H., Yesiloglu-Gultekin, N.J., 2017. Reliability-based stability analysis of rock slopes using numerical analysis and response surface method. Rock Mech. Rock. Eng. 50 (8), 2119–2133.
Dawson, E., Roth, W., Drescher, A., 1999. Slope stability analysis by strength reduction. Geotechnique 49 (6), 835–840.
Fan, Q., Zhu, H., Geng, J., 2015. Monitoring result analyses of high slope of five-step ship lock in the three Gorges Project. J. Rock Mech. Geotech. Eng. 7 (2), 199–206.
Fernandez Merodo, J., Mira, P., Pastor, M., Li, T., 1999. GeHoMadrid user manual. Internal Report, CEDEX, Madrid.
Firpo, G., Salvini, R., Francioni, M., Ranjith, P., 2011. Use of digital terrestrial photogrammetry in rocky slope stability analysis by distinct elements numerical methods. Int. J. Rock Mech. Min. Sci. 48 (7), 1045–1054.
Fookes, P.G., Sweeney, M., 1976. Stabilization and control of local rock falls and degrading rock slopes. Q. J. Eng. Geol. 9 (1), 37–55.
Griffiths, D., Lane, P., 1999. Slope stability analysis by finite elements. Geotechnique 49 (3), 387–403.
Griffiths, D., Marquez, R., 2007. Three-dimensional slope stability analysis by elasto-plastic finite elements. Geotechnique 57 (6), 537–546.
Hungr, O., Leroueil, S., Picarelli, L., 2014. The Varnes classification of landslide types, an update. Landslides 11 (2), 167–194.
Kilburn, C.R., Petley, D.N., 2003. Forecasting giant, catastrophic slope collapse: lessons from Vajont, Northern Italy. Geomorphology 54 (1–2), 21–32.
Li, D., Jiang, S., Cao, Z., Zhou, C., Li, X., Zhang, L., 2015. Efficient 3-D reliability analysis of the 530 m high abutment slope at Jinping I Hydropower Station during construction. Eng. Geol. 195, 269–281.
Ma, K., Tang, C., Liang, Z., Zhuang, D., Zhang, Q., 2017. Stability analysis and reinforcement evaluation of high-steep rock slope by microseismic monitoring. Eng. Geol. 218, 22–38.
Macfarlane, D., 2009. Observations and predictions of the behaviour of large, slow-moving landslides in schist, Clyde Dam reservoir, New Zealand. Eng. Geol. 109 (1–2), 5–15.
Paronuzzi, P., Bolla, A., 2012. The prehistoric Vajont rockslide: an updated geological model. Geomorphology 169, 165–191.
Soren, K., Budi, G., Sen, P., 2014. Stability analysis of open pit slope by finite difference method. Int. J. Res. Eng. Technol. 3 (5), 326–334.
Stead, D., Wolter, A., 2015. A critical review of rock slope failure mechanisms: the importance of structural geology. J. Struct. Geol. 74, 1–23.
Sun, K., Hu, C., 2007. Study on high rock slope for Xiluodu hydropower station's spandrel groove and water Iinlet. J. Yangtze River Sci. Res. Institut. 24 (2), 17–21.
Sun, J., Ning, Y., Zhao, Z., 2011. Comparative study of Sarma's method and the discontinuous deformation analysis for rock slope stability analysis. Geomech. Geoeng. 6 (4), 293–302.
Ureel, S., Momayez, M., 2014. An investigation of the limit equilibrium method and numerical modeling for rock slope stability analysis. In: Zhang, L., Wong, E.L.N.Y. (Eds.), Rock Mechanics and its Applications in Civil, Mining, and Petroleum Engineering. American Society of Civil Engineers, Reston, VA, pp. 218–227.
Varnes, D.J., 1978. Slope movement types and processes. In: Landslides Analysis and Control, 176, pp. 12–33.
Wang, F., Zhang, Y., Huo, Z., Matsumoto, T., Huang, B., 2004. The July 14, 2003 Qianjiangping landslide, three gorges reservoir, China. Landslides 1 (2), 157–162.
Wu, F., Luo, Y., Chang, Z., 2011. Slope reinforcement for housing in three Gorges reservoir area. J. Mt. Sci. 8 (2), 314.
Wyllie, D.C., Norrish, N.I., 1996. Stabilisation of rock slopes. In: Turner, A.K., Schuster, R.L. (Eds.), Landslides: Investigation and Mitigation. National Research Council, Transportation Research Board, Special Report 247, Washington, DC, pp. 474–504.
Xu, N., Wu, J., Dai, F., Fan, Y., Li, T., Li, B., 2018. Comprehensive evaluation of the stability of the left-bank slope at the Baihetan hydropower station in Southwest China. Bull. Eng. Geol. Environ. 77 (4), 1567–1588.
Yu, Y., Wang, E., Zhong, J., Liu, X., Li, P., Shi, M., Zhang, Z., 2014. Stability analysis of abutment slopes based on long-term monitoring and numerical simulation. Eng. Geol. 183, 159–169.
Zhang, J., He, J., Fan, J., 2001. Static and dynamic stability assessment of slopes or dam foundations using a rigid body–spring element method. Int. J. Rock Mech. Min. Sci. 38 (8), 1081–1090.
Zhu, H., Shi, B., Yan, J., Zhang, J., Wang, J., 2015. Investigation of the evolutionary process of a reinforced model slope using a fiber-optic monitoring network. Eng. Geol. 186, 34–43.
Zienkiewicz, O.C., Humpheson, C., Lewis, R., 1975. Associated and non-associated visco-plasticity and plasticity in soil mechanics. Geotechnique 25 (4), 671–689.